Synergetic Optimization Based on Doubly Salient Pole-Changing Machine for Torque Ripple Reduction

Wenjie Wu, Mingyuan Jiang, and Shuangxia Niu

Department of Electrical and Electronic Engineering, The Hong Kong Polytechnic University, Hong Kong, China

In order to achieve the objective of simultaneously reducing the torque ripple in different operating states, a synergetic optimization based on the double salient pole-changing machine is proposed. The key of this method is that make the theoretical analysis about the specific impact of torque ripple based on different parts of the proposed machine. This step can help to determine the main parameters that require to be optimized for torque ripple, and then, the surrogate model is built to represent the relationship between the parameters and torque ripple. Besides, the multi-objective optimization algorithm is applied to achieve the best torque ripple in different operating states. Finally, the optimized scheme is selected according to the optimization method and make the simulation to verify its effectiveness through the finite element analysis method.

Index Terms— **Flux-weakening capability, multi-auxiliary-teeth, pole-changing machine, zero-sequence current.**

I. Introduction

IN RECENT years, the prospects of doubly salient machine in application fields, such as electric vehicles, ship propulsion, and aircraft, have received widespread attention due to its higher torque density [1], [2], [3], [4], [5]. Compared with the permanent magnet vernier machine based on individual modulated teeth structure, the doubly salient structure has modulation teeth on both the stator and rotor sides. It means that the stator and rotor modulation teeth can generate and modulate more working harmonics based on the flux field modulation principle to generate the improved torque density.

However, except from the multiple working modulated harmonics, the doubly salient structure can also generate the non-working harmonics to increase the torque ripple. Therefore, its torque ripple is larger than other modulation machines. In order to decrease the torque ripple of the doubly salient machine, many feasible methods have been presented in [1], [6], [7], [8], and [9]. The six main feasible torque ripple reduction methods, including adding continuous skew rotor, step skew rotor, notching teeth, pairing structure, right-angle chamfering teeth, and cos-chamfering teeth, are widely used at present. In these six methods, adding the continuous skew rotor is the most effective method while it is hard to realize in actual manufactural process with the limited technology level. For adding the pairing structure, right-angle chamfering teeth, and cos-chamfering teeth, these three methods can reduce the torque ripple based on some specific slot–pole combinations. Nevertheless, these three methods may not achieve the desired torque ripple reduction effect for all the slot–pole combination. With regard to the step skew rotor and notching teeth, these two methods are most frequently used in doubly salient structure. It is because they are applicable to all the slot–pole combination and do not need the high technical requirements to manufacture. Therefore, these two methods are the main ways adopted in this article to reduce torque ripple.

Moreover, to better utilize the doubly salient machine in practical applications, the torque ripple under different operating states, not just in normal state, requires to be comprehensively considered and make further optimization. For doubly salient machines, in addition to torque density, the flux-weakening ability needs to be considered seriously. The better flux-weakening ability means a wider range of rotating speeds. At present, the pole-changing operation is widely used in the PM machine to improve the flux-weakening ability. It achieves the effect of speed expansion to weaken the flux field by changing the number of winding poles in the flux-weakening state.

At present, there are few articles that simultaneously focus on the torque ripple of doubly salient machines in normal operating states and flux-weakening states. The commonly used torque ripple reduction methods, such as adding step skew rotor and notching teeth, can usually only ensure a relatively small torque ripple in one state when used alone. It is difficult to simultaneously reduce torque ripple in both normal and flux-weakening states.

To overcome this problem, the step skew rotor and notching teeth are used simultaneously and in combination with each other in normal state and flux-weakening state. In addition, the imbalance of the excitation source during the pole changing operation can affect the torque ripple of the doubly salient machine. Therefore, the new added step skew rotor, notching teeth, and machine parameters that affecting the excitation sources are required to make the comprehensive optimization to reduce the torque ripples in normal state and flux-weakening state. In this article, a synergetic optimization method from three different perspectives is presented, which including skewing poles, notching teeth, and excitation sources. By analyzing the impact of these three parts on torque ripple, the machine parameters with significant influence are determined and selected. Moreover, the surrogate model with the

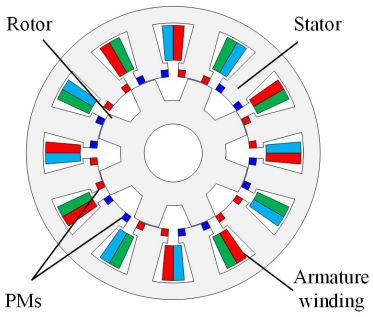

Fig. 1. Initial doubly salient structure.

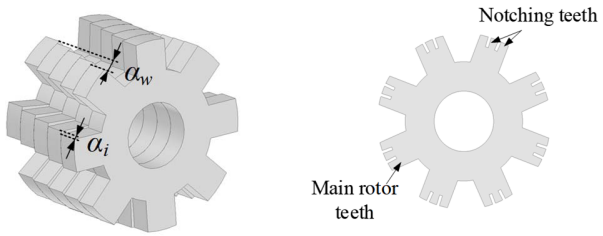

Fig. 2. Structure for torque ripple reduction. (a) Step-screwing rotor. (a) Notching teeth.

selected machine parameters and multi-objective optimization algorithm are applied to achieve the best torque ripple in different operating states.

II. Machine Configuration and Torque Ripple Analyses

A. Machine Configuration

The initial topological structure of the doubly salient machine is illustrated in Fig. 1. It can be seen that both the stator and rotor of this machine have modulation teeth. Based on the flux-field modulation theory, the rotor and stator modulation teeth can modulate the more working harmonics to improve its torque density. However, the doubly salient structure also makes the negative influence on the torque ripple because of the new modulated non-working harmonics based on the flux-field modulation effect.

For the sake of decreasing the torque ripple of this doubly salient PM machine and ensuring its stability of the rotational speed, the step-screwing structure is adopted to the rotor of the proposed machine, as shown in Fig. 2(a). The torque ripple of the proposed machine is mainly affected by the cogging torque. Before the adaptation of the step-screwing structure, it can be expressed as

$$T_{\text{cog}} = -\frac{\partial W_m}{\partial \alpha_m}\bigg|_{i=0} \tag{1}$$

where α_m is the rotor position and W_m is the magnetic energy of machine.

Because the permeability of the soft magnetic core is much greater than that of air. Meanwhile, it is assumed that the magnetic materials in the corresponding regions work in the linear region. The energy of the PM field can be expressed as follows:

$$\begin{aligned} W_m &= \frac{1}{2\mu_0}\int_V B_r^2(\theta,\alpha_m)dV \\ &= \frac{1}{2\mu_0}\int_V B_r^2(\theta)G_n^2(\theta,\alpha_m)dV \\ &= \frac{1}{2\mu_0}\int_V B_r^2(\theta)\left[\frac{h_m(\theta)}{h_m(\theta)+\delta(\theta,\alpha_m)}\right]^2 dV \end{aligned} \tag{2}$$

where μ_0 is the permeability of vacuum, B is the air-gap magnetic density, θ is the angle along the rotor rotation direction, $B_r(\theta)$ is the remanence of the excitation source, $G_n(\theta,\alpha_m)$ is the relative air-gap permeance, $\delta(\theta,\alpha_m)$ is the effective air-gap length at different positions along the circumference, and $h_m(\theta)$ is the length of magnets in the magnetization direction.

Through decomposing the Fourier function of $B_r(\theta)$ and $G_n(\theta,\alpha_m)$, their specific Fourier expansions can be expressed as

$$\begin{aligned} B_r^2(\theta) &= B_{r0} + \sum_{n=1}^{\infty} B_{rn}\cos 2np\theta \\ &= \alpha_p B_r^2 + \sum_{n=1}^{\infty}\frac{2}{n\pi}B_r^2 \sin n\alpha_p\pi \cos 2np\theta \end{aligned} \tag{3}$$

where B_{r0} is the initial component of the $B_r(\theta)$, B_{rn} is the Fourier decomposition coefficient of excitation source remanence, α_p is the pole arc coefficient, and p is the pole-number number of the excitation source

$$\begin{aligned} G_n^2(\theta,\alpha_m) &= \left[\frac{h_m(\theta)}{h_m(\theta)+\delta(\theta,\alpha_m)}\right]^2 \\ &= G_0 + \sum_{n=1}^{\infty} G_n \cos nZ(\theta+\alpha_m) \end{aligned} \tag{4}$$

where G_0 is the constant part of $G_n^2(\theta,\alpha_m)$, G_n is the Fourier coefficient of the square component of the relative air-gap permeability, and Z is the number of the stator slots.

Substituting (2)–(4) into (1), the specific cogging torque equation of the doubly salient machine without the step-screwing can be presented as follows:

$$T_{\text{cog}}(\alpha) = \frac{\pi L\left(R_2^2 - R_1^2\right)}{4\mu_0}\sum_{n=1}^{\infty} iG_nB_r \sin k_{mn}\alpha \tag{5}$$

where L is the axial stack length, R_1 and R_2 are the inner and outer air-gap radius, respectively, and k_{mn} is the least common multiple of N_s and N_e.

From Fig. 2(a), the step-screwing rotor is evenly divided into n segments in the axial direction, and the angle between two axial adjacent segments is $\alpha_w = \alpha_i\ (n-1)$. The cogging torque of the whole step-skewing rotor can be written as

$$\begin{aligned} T_{\text{cog}}(\alpha) &= \frac{\pi L\left(R_2^2 - R_1^2\right)}{4\mu_0 n} \\ &\times \sum_{n=1}^{\infty} iG_nB_r \frac{\sin\frac{k_{mn}\alpha_w}{2}\frac{n}{n-1}}{\sin\frac{k_{mn}\alpha_i}{2}} \sin k_{mn}\left(\alpha+\frac{\alpha_w}{2}\right). \end{aligned} \tag{6}$$

Compared (5) and (6), it can be determined that the cogging torque is smaller with the help of the step-screwing rotor.

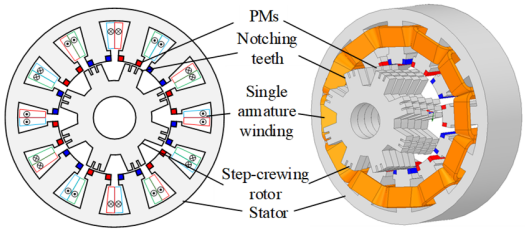

Fig. 3. Structure for torque ripple reduction with step-screwing rotor and notching teeth.

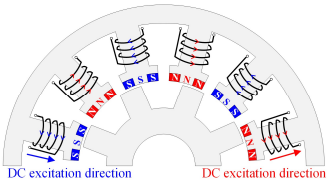

Fig. 4. Polarity of excitation flux field in normal state.

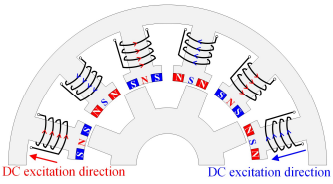

Fig. 5. Polarity of excitation flux field in the flux-weakening state.

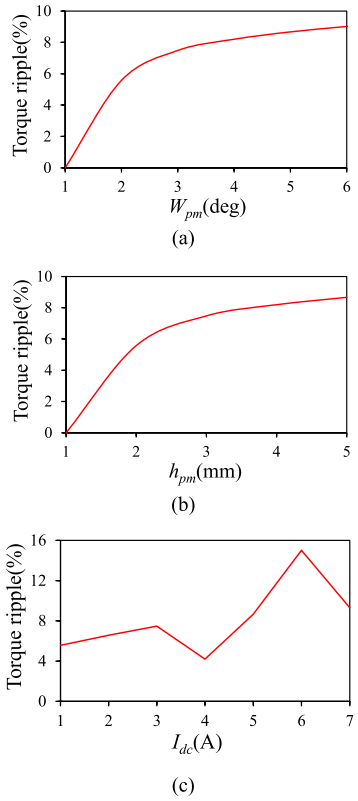

Fig. 6. Influence of the excitation source parameters about the torque ripple. (a) W_{pm} versus torque ripple. (b) h_{pm} versus torque ripple. (c) I_{dc} versus torque ripple.

Moreover, in order to ensure the smooth operation of the proposed machine in both flux-enhancing state and flux-weakening state, the notching structure is also applied to the rotor to further reduce the torque ripple. This structure in Fig. 2(a) is able to change the amplitude and phase of modulated harmonics, which is conductive to suppress torque ripple. The topological structure with the step-screwing rotor and notching teeth is illustrated in Fig. 3.

B. Influence of the Excitation Source Flux Field Balance

In addition to the newly added structure, the flux field balance of this doubly salient machine will affect the torque ripple. To improve the flux-weakening ability, the zero-sequence current is injected as the additional dc excitation source to adjust and weaken the flux field of this doubly salient structure. Through changing the direction of the zero-sequence current, the flux-weakening state is realized to transform the polarity of the excitation flux field, thereby realizing the objective of the flux-weakening improvement. Figs. 4 and 5 show the polarity of excitation flux field in different states. It can be seen that the PM flux field is determined by the parameter of the PMs, while the flux field generated by dc excitation source is determined by the value of the dc current. When the dc current is injected with the undesirable value, the PM flux field and dc excitation flux field are likely to be unbalanced. It means that the unbalanced dc and PM excitation source modulated by the doubly salient structure can generate the more non-working harmonics to make the negative influence on torque ripple. Fig. 6 shows the influence of the PM parameters about the PM excitation source and injected dc current of dc excitation source. It can be seen that these variations can influence the torque ripple significantly. Therefore, the balance of the PM and dc excitation source is important to be considered to reduce the torque ripple.

III. Synergetic Optimization Method

A. Overall Optimization Process

Fig. 7 presents the overall synergetic optimization process. It is shown that the proposed optimization method can be divided into three main parts, which can be involved as follows.

1) *Skewing Poles Optimization:* The step skewing rotor is applied and optimized to reduce the cogging torque. According to the analysis in Section II, the angle a_i between two axial adjacent segments and the overall tilt angle a_w are the main parameters to influence the torque ripples in normal and flux-weakening states.
2) *Notching Teeth Optimization:* The notching teeth is arranged and optimized on main rotor modulation teeth to adjust the flux field harmonic amplitude and phase. For this structure, the width w_n and height h_n of the notching teeth are the determined parameters to make the positive influence on the torque ripple reduction.
3) *Excitation Sources Optimization:* Through the analysis in Section II, the PM and dc excitation source requires to be optimized to ensure the balance of the excitation source flux field. The value of the injected dc current I_{dc}, the width w_m of PMs, and width w_s of the stator teeth mainly affect the PM and dc excitation source.

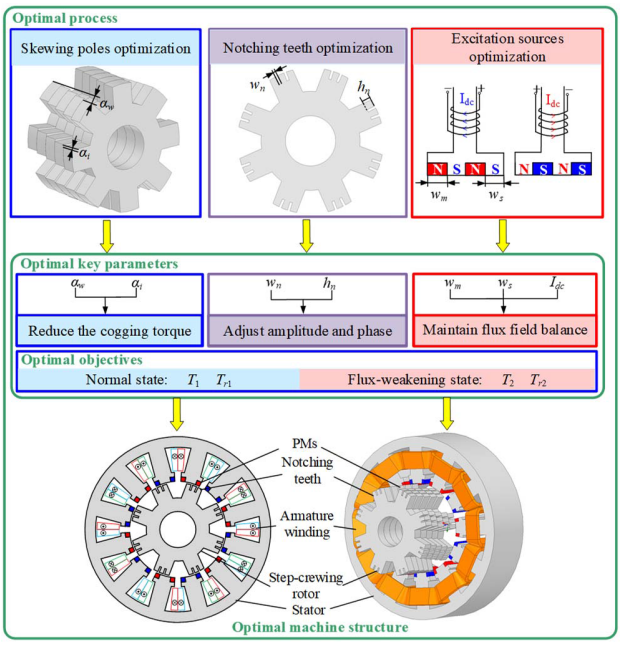

Fig. 7. Process of the proposed synergetic optimization method.

Therefore, these three parameters are selected to ensure the balance between the excitation source.

Apart from these selected design parameters, the optimal objectives also require to be selected. In this article, the values of the average torque and torque ripple in normal and flux-weakening states are selected as the optimal objectives, respectively. Specifically, in order to reduce the number of optimization objectives and improve the convergence and accuracy of the optimization model, the torque ripple under different states is set as constrained conditions. The constrained model has the form as

$$\begin{aligned} &\text{Objectives: } \mathrm{Max}[T_1], \mathrm{Max}[T_2] \\ &\text{Constraints: } T_{r1} \le 15\%, \quad T_{r2} \le 15\% \\ &\boldsymbol{x} \in \{I_{\mathrm{dc}}, w_s, w_n, w_m, h_n, \alpha_i, \alpha_w\}. \end{aligned} \tag{7}$$

B. Surrogate Model

Based on (7), the relationship between machine parameter variables and optimal objectives can be expressed. To significantly reduce model analysis time and improve optimization efficiency, the generalized neural network (GRNN) model is applied to express these relationships, as shown in Fig. 8.

The surrogate model constructed using GRNN has the advantages of strong nonlinear mapping ability and fast self-learning ability, which can significantly reduce model analysis time and improve optimization efficiency [10], [11].

Due to the high dimensionality of the seven parameters that need to be optimized for this machine, a large number of sampling points are required to establish a surrogate model. Compared with the traditional surrogate model like response surface model, GRNN model has stronger approximation ability and learning speed, requiring fewer sampling points to achieve the same fitting accuracy. Moreover, the optimal objective of the torque ripple is greatly affected by variation of

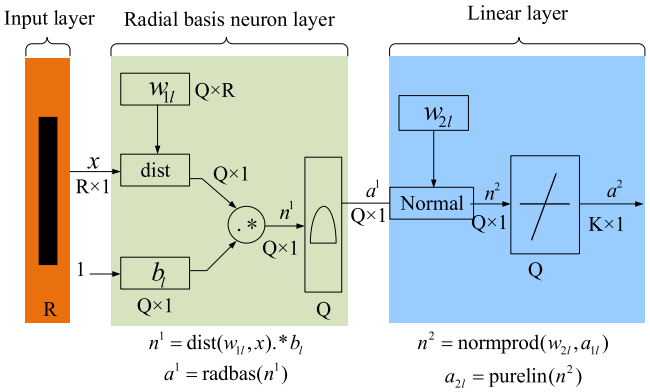

Fig. 8. Flowchart of the GRNN.

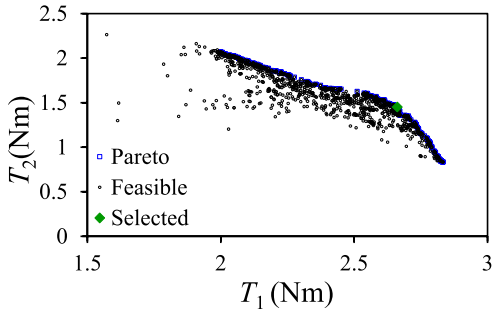

Fig. 9. Final optimization results.

the optimization parameters. GRNN model is more facilitated to ensure the accuracy of the relationship.

Therefore, in order to improve the efficiency of establishing optimization models, this article uses GRNN network to establish the surrogate model, characterizing the relationship between motor parameter variables and output performance, providing optimization space for subsequent operation of optimization algorithms.

C. Optimization Result

Based on the established model, the multi-objective optimization algorithm is used in this article to achieve and select the optimal solution [12], [13], [14]. Fig. 9 shows the optimization results of the proposed machine. The black points are the feasible schemes, which satisfy the constrained condition. The blue points are the pareto fronts by optimization method, where the green points are selected as the final optimization result to conduct further performance comparison.

Fig. 10(a) and (b) shows the air-gap flux harmonic distribution in the normal and flux-weakening states, respectively. The working harmonics are those components with the black marks. It can be seen that the optimized scheme has the less non-working harmonics when conducting the optimization method. Therefore, the torque ripples of the optimized scheme in normal and flux-weakening states are both reduced. Fig. 11 compares the simulated torque waveforms in different operating states between the original and optimized schemes. It is illustrated that the optimized torque ripple in normal state is about 15%, reducing from 30% for the original scheme. Moreover, the torque ripple in flux-weakening state

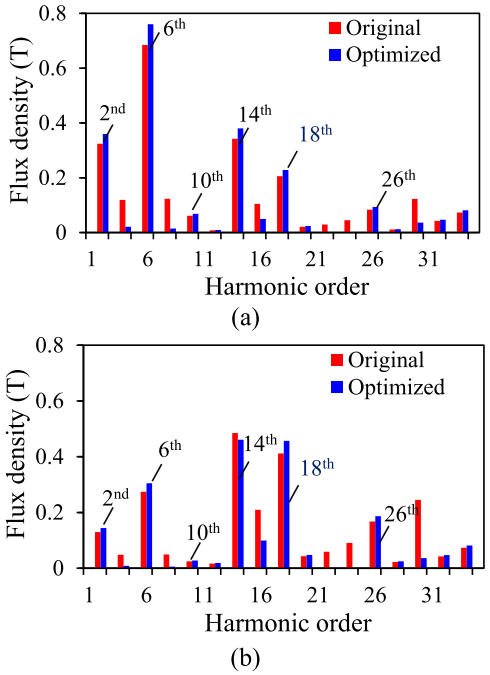

Fig. 10. Air-gap flux harmonic distribution. (a) Normal state. (b) Flux-weakening state.

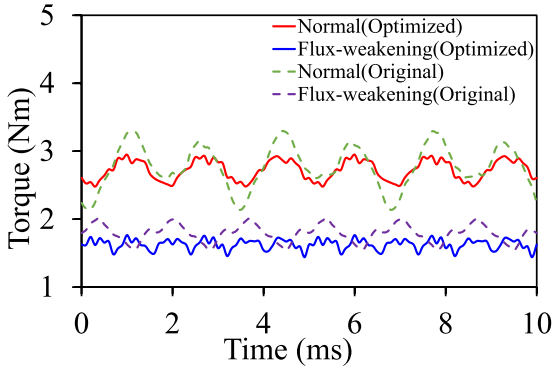

Fig. 11. Waveforms of torque performance.

decreases from 20% of the original scheme to 10% of the optimized scheme when performing the optimization method. This simulated result verifies the effectiveness of the proposed synergetic optimization method.

IV. Conclusion

In this article, a synergetic optimization based on doubly salient pole-changing machine is proposed to reduce the torque ripple in different operating states. The proposed optimization method has the characteristics of high optimization efficiency and accurate optimization precision. First, the part that has the greatest impact on torque ripple is analyzed based on flux field modulation theory, in order to determine the main optimization parameters. Moreover, the optimization model is built and the algorithm is applied to the doubly salient machine to optimize performance parameters with the best torque performance. In order to reduce computational time, the surrogate models are applied to the optimization process to improve optimization efficiency. Finally, the electromagnetic torque performance of the doubly salient machine after synergetic optimization method is analyzed and compared with the original scheme to present the effectiveness of the proposed optimization method.

Acknowledgment

This work was supported in part by the National Natural Science Foundation of China under Project 52077187; and in part by the Research Grant Council, Hong Kong, China, under Project Polyu 152109/20E.

References

[1] L. Wu, G. Ming, L. Zhang, and Y. Fang, "Improved stator/rotor-pole number combinations for torque ripple reduction in doubly salient PM machines," *IEEE Trans. Ind. Electron.*, vol. 68, no. 11, pp. 10601–10611, Nov. 2021.

[2] H. Cheng, F. Lin, C. Peng, J. Sun, and J. Chu, "Development and optimization design of a novel double stator doubly salient variable flux memory motor," *IEEE Trans. Energy Convers.*, vol. 39, no. 4, pp. 2134–2145, Dec. 2024, doi: 10.1109/TEC.2024.3384512.

[3] X. Chen, Z. Zhang, L. Yu, Y. Sun, and Q. Xu, "A variable sampling-frequency-based commutation delay compensation method for high-speed doubly salient motor considering speed fluctuation," *IEEE Trans. Ind. Electron.*, vol. 71, no. 9, pp. 10221–10234, Sep. 2024.

[4] F. Ni, S. Niu, Z. Li, and X. Zhao, "Novel electrically excited doubly salient variable reluctance machine with high-order-harmonic winding," *IEEE Trans. Magn.*, vol. 59, no. 11, Nov. 2023, Art. no. 8101906.

[5] L. Yu, W. Chen, Q. Xu, Z. Zhang, and Y. Shi, "Reduction of cross-coupling for bearingless doubly salient electromagnetic motor using nonsynchronous rotating coordinate transformation," *IEEE Trans. Ind. Electron.*, vol. 70, no. 8, pp. 7706–7715, Aug. 2023.

[6] Z. Yu, C. Gan, K. Ni, Y. Chen, and R. Qu, "Instantaneous torque modeling and torque ripple reduction strategy for flux modulated doubly-salient reluctance motor drives," *IEEE Trans. Ind. Electron.*, vol. 69, no. 10, pp. 9838–9848, Oct. 2022.

[7] C. H. T. Lee, K. T. Chau, C. Liu, T. W. Ching, and F. Li, "Mechanical offset for torque ripple reduction for magnetless double-stator doubly salient machine," *IEEE Trans. Magn.*, vol. 50, no. 11, pp. 1–4, Nov. 2014.

[8] Z. Yu, C. Gan, K. Ni, Y. Chen, and R. Qu, "Analytical torque ripple reduction strategy for flux modulated doubly-salient reluctance motor drives based on ZSC harmonic regulation," *IEEE Trans. Ind. Electron.*, vol. 71, no. 2, pp. 1365–1376, Feb. 2024.

[9] G. J. Li, K. Zhang, Z. Q. Zhu, and G. W. Jewell, "Comparative studies of torque performance improvement for different doubly salient synchronous reluctance machines by current harmonic injection," *IEEE Trans. Energy Convers.*, vol. 34, no. 2, pp. 1094–1104, Jun. 2019.

[10] M. Tahkola, V. Mukherjee, and J. Keränen, "Transient modeling of induction machine using artificial neural network surrogate models," *IEEE Trans. Magn.*, vol. 58, no. 9, pp. 1–4, Sep. 2022, doi: 10.1109/TMAG.2022.3180176.

[11] J. Gu, W. Hua, W. Yu, Z. Zhang, and H. Zhang, "Surrogate model-based multiobjective optimization of high-speed PM synchronous machine: Construction and comparison," *IEEE Trans. Transport. Electrific.*, vol. 9, no. 1, pp. 678–688, Mar. 2023.

[12] Y. Ma, J. Wang, L. Zhou, and K. Shuai, "Surrogate-assisted optimization of a five-phase SPM machine with quasi-trapezoidal PMs," *IEEE Trans. Ind. Electron.*, vol. 69, no. 1, pp. 202–212, Jan. 2022, doi: 10.1109/TIE.2020.3048279.

[13] L. Xu, W. Wu, and W. Zhao, "Airgap magnetic field harmonic synergetic optimization approach for power factor improvement of PM Vernier machines," *IEEE Trans. Ind. Electron.*, vol. 69, no. 12, pp. 12281–12291, Dec. 2022.

[14] L. Xu, W. Wu, W. Zhao, G. Liu, and S. Niu, "Robust design and optimization for a permanent magnet Vernier machine with hybrid stator," *IEEE Trans. Energy Convers.*, vol. 35, no. 4, pp. 2086–2094, Dec. 2020.